Propagation of Femtosecond Surface Plasmon Polariton Pulses on the Surface of a Nanostructured Metallic Film: Space-Time Complex Amplitude Characterization

R. Rokitski,* K. A. Tetz,† and Y. Fainman

Department of Electrical and Computer Engineering, University of California, San Diego, La Jolla, California 92093-0409, USA

(Received 29 April 2005; published 18 October 2005)

Ultrashort surface plasmon polariton (SPP) pulses, propagating on the surface of a nanostructured metallic film, are characterized in space and time using time-resolved spatial-heterodyne imaging. Optical pulses are coupled from free space into various surface modes using a 2D array of circular nanoholes, and spatial amplitude and phase characteristics of the scattered surface field are measured with femtosecond-scale time resolution. Demonstrated in-plane focusing of SPP pulse provides additional electromagnetic field localization with possible applications in SPP nanophotonics, nonlinear surface dynamics, biochemical sensing, and ultrafast surface studies.

DOI: 10.1103/PhysRevLett.95.177401 PACS numbers: 78.67.−n, 42.25.Bs, 42.40.Kw, 78.47.+p

Photonic modes at the interface between metallic and dielectric materials possess unique properties that arise due to the coupling to plasmon modes in the metal layer. These coupled modes, surface plasmons or surface plasmon polaritons (SPPs), exhibit intrinsic field localization at the interface between the media that facilitates waveguiding and reduces average power requirements for nonlinear wave mixing. These unique features of surface plasmon polaritons could lead to SPP-based photonic devices that are much more compact than those currently achievable with optical refraction technologies and possibly bridge the gaps between photonics, biochemical sensing and CMOS-based electronics technologies. The fundamental properties of surface plasmon polariton waves have been a subject of intensive study [1]. Recent interest in this area sparked with the discovery of extraordinary light transmission through nanohole arrays [2,3] and the role of SPPs in this process. In these studies one and two-dimensional periodic structures are used to couple to surface plasmon modes, and the majority of experimental measurements have consisted of steady-state spectral and angular transmission and reflection properties of both single holes and hole arrays. Most of the time-resolved studies of SPPs [4–6] have focused on space-averaged characteristics of light reflected from or transmitted through corrugated metallic surfaces, while a few efforts [7] have investigated propagation of femtosecond pulses along the metal surface. Comprehensive investigation of SPP evolution along the propagation direction was beyond experimental capability. Many potential applications of SPPs for information transmission, processing and detection, however, would require complete understanding of the in-plane SPP pulse propagation. This requires experimental characterization of SPP amplitude and phase evolution upon propagation, which presents an unexplored challenge on the way to building practical plasmonic devices for future information technologies.

In this work we investigate the excitation and propagation of femtosecond SPP pulses using a time-resolved version of the spatial-heterodyne imaging technique, which provides the spatial distributions of the electromagnetic field amplitude and phase versus time. This method has successfully been applied in various research areas ranging from fiber optics to plasma physics [8,9]. Since the SPP field stays bound to the metal surface in the absence of surface defects, the field may be observed through evanescent coupling in the near zone or must be converted to radiating modes at the desired spatial locations. In our experiment the optical field is coupled into and out of the metallic film using a single array of nanoholes etched in the metallic film. We observe excitation and scattering of femtosecond SPP pulses in 100 nm thick aluminum films, deposited on a GaAs substrate and perforated with an array of circular nanoholes. The holes with diameter 350 nm are distributed uniformly on the square grid with total array size $200 \times 200\ \mu\text{m}^2$. Results are presented for arrays with hole periods $a = 1.4$ and $1.6\ \mu$m. To characterize SPP resonance excitation, we developed a dispersion map of the nanohole array by measuring the spectral transmittance as a function of in-plane wave vector [2,10] for the Γ-M and Γ-X directions. The data, combining measurements of both arrays and presented in Fig. 1, are dominated by asymmetric line shape features [11,12], which correlate with resonance transmission by excitation of SPP waves—in this case on a single interface. For our samples, only SPP modes on the metal-air interface are efficiently excited; the first order modes for the semiconductor-air interface occur at much lower frequencies, and the higher order modes that occur at these frequencies are not discernible in our measurements.

Imaging of SPP modes is performed using a modified Mach-Zehnder interferometer. Optical pulses with central wavelength 1550 nm and temporal width FWHM $\approx$ 200 fs are derived from a mode-locked laser and focused in the center of the nanohole array with 5× and 10× microscope objectives through the substrate at normal incidence angle (Fig. 2). The sample is placed between two crossed polar-

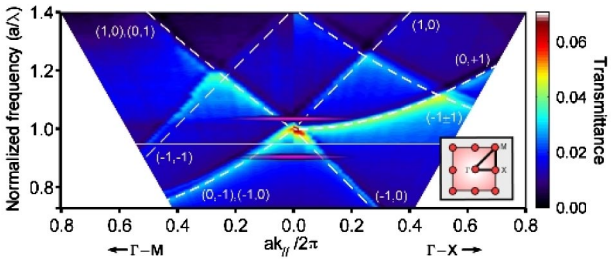

FIG. 1 (color online). Measured transmittance of nanohole arrays superimposed with calculated dispersion map of SPP modes. Transmittance is displayed in false color as a function of normalized frequency versus normalized in-plane wave vector measured in two directions (as indicated in reciprocal space diagram in inset). Data for two different grating periods, $a = 1.4\ \mu$m (top) and 1.6 μm (bottom), are combined to show the whole parameter space, with the stitching between data sets occurring at the horizontal, solid white line. Phase matching conditions are displayed for a SPP on an air-aluminum interface with dashed white lines. Pink ellipses represent the incident femtosecond pulse for the two arrays under study: in frequency limited by the pulse spectral bandwidth and in wave vector by the angular intensity distribution of the illumination beam. The interplay between the spectral and angular bandwidths of the incident optical pulse is similar to the phase matching effects observed in volume holography and nonlinear optics.

izers, blocking light transmitted directly through the film at the excitation point. The polarizer-analyzer pair is oriented at 45° with respect to the array axes providing polarization projection of the incident optical field in the direction of the SPP polarization [13,14]. We identify the optical field observed on the other side of the array as scattered SPP field (as opposed to diffracted and scattered free-space mode) by confirming, consistently with [13], its polarization state along the propagation direction in the metal surface. This optical field is collected with a 20× micro-

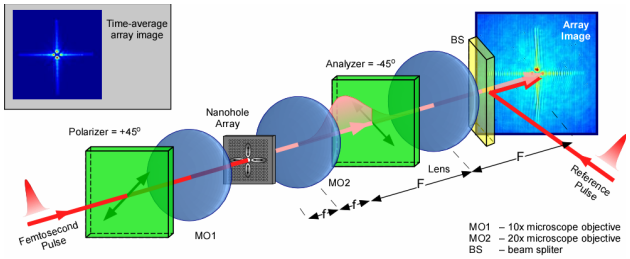

FIG. 2 (color online). Schematic diagram for excitation and time-resolved imaging of femtosecond surface plasmon polariton (SPP) pulses. The nanohole array ($200 \times 200\ \mu$m^2 size is greatly exaggerated) is imaged with 40 times magnification on the CCD surface, where the optical field, radiated by propagating SPP pulse forms interference with a superimposed femtosecond reference pulse. The interference pattern is shown in false color for $\Delta\tau = 0.5$ ps delay between the pulses. A crossed polarizer-analyzer pair is used to block the directly transmitted optical field while passing the scattered SPP field. Inset figure shows time-average scattered SPP field, detected without reference femtosecond pulse.

scope objective and imaged with a $4f$ optical arrangement onto the surface of InGaAs digital camera. Temporal gating of the collected optical field is performed using a time-resolved spatial-heterodyne imaging technique. The reference optical pulse, derived from the same laser, is combined with the scattered femtosecond SPP pulse on the surface of the CCD in holographic recording configuration, and the resulting interference pattern is measured as a function of relative delay between the scattered SPP and reference fields. We process each measured interference pattern to obtain spatial amplitude and phase distributions for each position of the delay.

The scattered SPP field, observed in the absence of the time-gating reference optical field, is shown in Fig. 2. Four lobes of the observed field correspond to $(1, 0)$ and $(0, 1)$ SPP modes propagating from the center to the edges of the array along the array's x and y axes. Since the SPP is efficiently coupled out from the metal surface only in the corrugation region, the scattered SPP field is not observed outside of the array. Exponential decay of each lobe towards the edges of the array demonstrates that upon propagation the surface field experiences attenuation of $\sim 20\ \mu$m^{-1} due to both material absorption and scattering losses. This value is consistent with our detailed attenuation measurements of SPPs, propagating on nanohole array surface and obtained with cw illumination [14,15]. Cross sections of a single lobe display nearly Gaussian spatial mode profiles.

In the presence of a short time-gating optical pulse the camera detects interference between the scattered femtosecond SPP pulse and the reference pulse when they overlap in time and space. A typical interference pattern observed for ~0.5 ps delay between the signal and the reference is shown in Fig. 2 in the array image plane. Vertical interference fringes demonstrate that the spatial-heterodyne frequency is oriented horizontally, along the k_x direction. Time-resolved spatial-heterodyne data are intrinsically sheared in the direction of the spatial carrier frequency, and for proper space-time data presentation we performed 3D unshearing of the measured data. Horizontal orientation of the spatial-heterodyne frequency provides suboptimal spatial resolution; however, this configuration greatly simplifies time-space unshearing of the measured data. Since the interference is observed only when the signal and the reference fields overlap in time, scanning of the delay between the scattered SPP and the reference field allows tracking the evolution of the SPP field with time. The measured signal corresponds to a temporal optical field cross correlation of the SPP waveform with the reference short pulse waveform.

The images shown in Figs. 3(a)–3(d) represent spatial amplitude distributions at 4 different delays between the interfering fields: $\Delta\tau = 0$, 133, 266, and 400 fs for the sample with array period 1.6 μm and 5× illumination objective. All the measured data frames are combined into a movie with ~1 ps total duration and ~3 fs frame separation. In the movie we observe in real time how four

SPP short pulses are first excited in the center and then propagate towards the edges of the array. Since the SPP pulses experience attenuation, their intensity significantly reduces upon propagation. A close look at the spatial amplitude distributions at short time delays [Figs. 3(a) and 3(b)] reveals significant spatial amplitude modulation of the field, which is absent at longer time delays [Figs. 3(c) and 3(d)]. We attribute this amplitude modulation to spatial interference of four femtosecond SPP pulses, propagating towards the center of the SPP excitation region. At the short time delays four excited SPP pulses overlap spatially and temporally in the center of the array. Their fields sum up coherently with appropriate phases to form the observed SPP modal interference pattern. At longer delays the pulses pass through the center, separate spatially, and no interference is observed.

The temporal evolution is characterized by measuring the cross correlation of the scattered SPP and reference optical fields at different spatial locations along the propagation path. The results of this measurement are shown in Fig. 3(e) for three spatial locations separated by $\sim 25\ \mu$m. The peak amplitude of the SPP pulse decays exponentially while the waveform maintains nearly the same shape. The ratio of the spatial location over the waveform delay gives an estimate of SPP pulse group velocity $\sim 300\ \mu$m/ps, which is equal to the speed of light in vacuum within the accuracy of our experiment and agrees with the fact that the observed SPP mode propagates along metal-air interface with the evanescent electromagnetic field concentrated in the air.

Spatial phase information of the propagating femtosecond SPP field was investigated in two nanohole arrays with

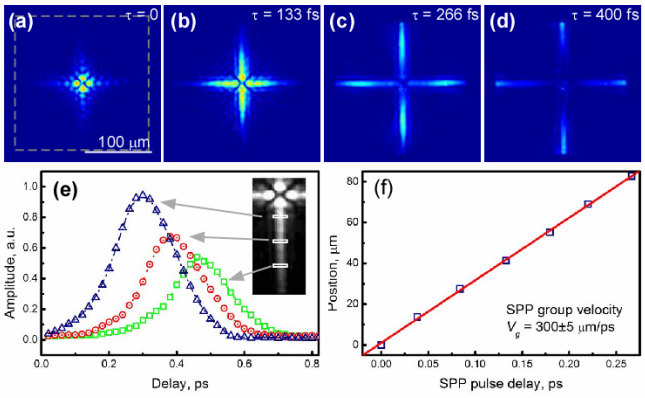

FIG. 3 (color online). Temporal evolution of scattered femtosecond SPP pulse. (a)–(d) Spatial amplitude of the femtosecond SPP pulse (shown in false color) scattered from nanohole array with $a = 1.6\ \mu$m hole period, measured for several time delays between SPP and reference pulses. (e) Normalized temporal cross correlation of scattered SPP and reference pulses, measured at three spatial locations along the SPP propagation path. (f) Delay of the SPP pulse peak measured at different positions along the propagation path gives SPP pulse group velocity $\sim 300 \pm 5\ \mu$m/ps. Dashed line in (a) outlines dimensions of the nanohole array.

hole periods $a = 1.4$ and $1.6\ \mu$m, supporting $(-1, 0)$, $(0, -1)$ and $(1, 0)$, $(0, 1)$ SPP modes with our illumination conditions, as indicated in the phase matching diagram in Fig. 1. Nanohole arrays were illuminated with converging and diverging Gaussian beams using a $10\times$ microscope objective. Measured spatial amplitude and phase distributions are presented in Figs. 4(a)–4(d) for a fixed delay between the scattered SPP field and the reference femtosecond pulse. Spatial amplitude distributions of the scattered SPP field show that when the nanohole arrays are illuminated with a converging Gaussian beam, the excited surface field continues converging and focuses—as clearly seen in Figs. 4(a) and 4(c). The opposite effect is observed when the arrays are illuminated with diverging Gaussian beams—the surface field diverges within the metal surface from the illumination point, as shown in Figs. 4(b) and 4(d) and the amplitude decays accordingly. Complete information about surface plasmon polaritons converging and diverging in the plane of nanohole arrays is provided in 4 movies, corresponding to Figs. 4(a)–4(d) and showing

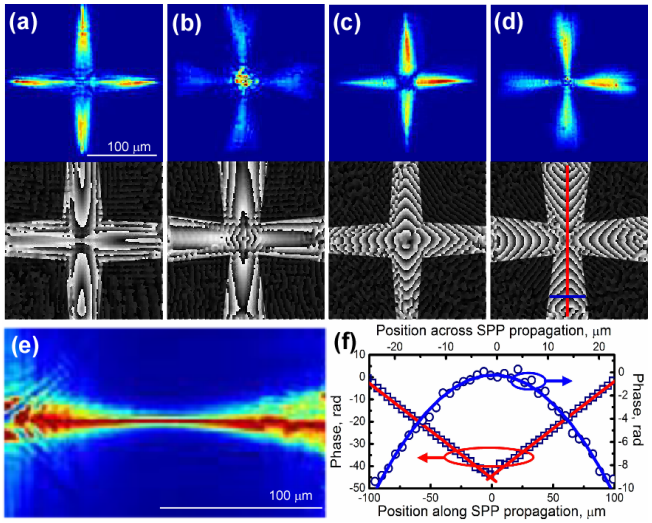

FIG. 4 (color online). Spatial evolution of scattered SPP field. (a)–(d) Spatial amplitude and phase (modulo 2π) distributions of scattered SPP pulse measured with 1.6 μm (a),(b) and 1.4 μm (c),(d) nanohole array periods with converging (a),(c) and diverging (b),(d) Gaussian beam illumination showing SPP field focusing and defocusing within the metallic film surface. Red and blue lines in phase distribution (d) show direction of cross sections for phase plots in (f). Spatial phase distributions demonstrate direct (a),(b) and inverse (c),(d) phase relationship between incident optical field and scattered SPP field. (e) In-plane SPP focal waist formation, measured in nanohole array with 1.6 μm period. Amplitude is renormalized in SPP propagation direction (horizontal) to compensate for attenuation. (f) Unwrapped longitudinal (open squares) and transversal (open circles) cross sections of the spatial phase distribution from (d) with linear and quadratic least-squares fitting plots. Linear phase corresponds to 6.0° phase matching angle for $(-1, 0)$ and $(0, -1)$ SPP modes shown in Fig. 1, while the quadratic spatial phase of the SPP field is acquired from the quadratic spatial phase of the incident optical field.

this effect in real time. The amplitude of the scattered femtosecond SPP pulse in the movies was rescaled with a gamma factor of 1.5 for better observation. To visualize propagation of the femtosecond pulse through the waist of the focused surface field we excite an SPP field on the edge of the array and measure its propagation for a distance of 200 μm [Fig. 4(e)]. Time-average amplitude of the observed field was rescaled at each position along the propagation path (in the horizontal direction) to compensate for longitudinal attenuation and clearly show transversal spatial transformation of the surface field. The measured width of the SPP waist of $2w_0 \approx 4$ μm is determined by the diffraction limit of our imaging system. An alternative method for focusing SPPs has recently been demonstrated using surface optical elements [16]. We note that while the surface field reaches maximum spatial localization (i.e., minimal transverse field profile) at the focal point, the absolute field intensity is reduced due to attenuation.

Spatial phase distributions in Figs. 4(a)–4(d) show several characteristic features of the scattered SPP fields. For both nanohole arrays vertical cross section of the spatial phase profile shows linear phase variation along the SPP propagation path up and down from the excitation point [Fig. 4(f)]. The amount of this linear phase directly corresponds to the incidence angle of the free-space optical wave most efficiently coupled with SPP. As we expected, the magnitude of the linear phase is the same for both converging and diverging beam illumination and corresponds to the radiation angles of $\sim 6.4°$ and $\sim 1.2°$ for arrays with 1.4 and 1.6 μm nanohole periods, respectively. These measured values are consistent with the expected phase matching angles 6.0° and 1.9°, observed in the Fig. 1 at the overlap regions of pink ellipses and dashed white lines. Transversal phase distributions for both arrays demonstrate close to quadratic profiles [Fig. 4(f)], implying converging and diverging propagation of the surface field; however, the signs of the quadratic phase are opposite for the two arrays. While scattered $(0, 1)$ and $(1, 0)$ SPP modes have positive wave-front curvature [see Figs. 4(a) and 4(b)], normal for Gaussian beams in free space, the field of scattered $(-1, 0)$ and $(0, -1)$ SPP modes demonstrates in Figs. 4(c) and 4(d) negative curvature of the spatial phase front with respect to the waist of the focused SPP. Additionally, the movies corresponding to Figs. 4(c) and 4(d) demonstrate opposite propagation direction for the surface field amplitude and phase: while the amplitude propagates from the center to the edges of the array, the spatial phase converges to the SPP excitation point. This counterintuitive phase behavior for $(-1, 0)$ and $(0, -1)$ SPP modes can be understood by looking at the phase matching conditions for SPP excitation. The negative sign in the notation of these SPP modes indicates the projection of the incident wave vector opposite to the SPP wave vector. The wave front of the SPP is reversed with respect to the incident wave and the propagation direction of the excited SPP field is opposite to the direction of the incident optical wave.

Excitation and observation of femtosecond surface plasmon polariton pulses using time-resolved spatial-heterodyne imaging approach is an important step towards understanding the relationship between spatial and temporal characteristics of the incident optical waves and the excited and scattered femtosecond SPP fields. Spatial resolution may be improved in the future using time-resolved heterodyne near-field imaging [17–19] to reveal nanoscale properties of the surface field. Demonstrated in-plane focusing of femtosecond SPP pulses leads to complete 3D and temporal localization of electromagnetic field, which will find applications in nonlinear surface studies, sensing surface plasmon polariton waveguiding and information processing. Because of the optical field correlation nature of our measurements, only spatial amplitude and phase information of the SPP field can be measured precisely. We envision, however, two-photon absorption realization of our measurements with the possibility of characterizing the temporal amplitude and phase of the femtosecond surface plasmon polariton pulses.

We thank the National Science Foundation, the Air Force Office of Scientific Research, and The Defense Advanced Research Projects Agency for financial support.

*Electronic address: rokitski@ucsd.edu
†Electronic address: ktetz@ucsd.edu

[1] H. Raether, *Surface Plasmons* (Springer-Verlag, Berlin, 1988).
[2] T. W. Ebbesen *et al.*, Nature (London) **391**, 667 (1998).
[3] W. L. Barnes, A. Dereux, and T. W. Ebbesen, Nature (London) **424**, 824 (2003).
[4] A. Dogariu *et al.*, Opt. Lett. **26**, 450 (2001).
[5] Yu. E. Lozovik *et al.*, JETP Lett. **75**, 9 (2002).
[6] Y.-H. Liau, S. Egusa, and N. F. Scherer, Opt. Lett. **27**, 857 (2002).
[7] M. Van Exter and A. Lagendijk, Phys. Rev. Lett. **60**, 1 (1988).
[8] R. Rokitski, P.-C. Sun, and Y. Fainman, Opt. Lett. **26**, 1125 (2001).
[9] M. Centurion, Y. P. Zhiwen Liu, D. Psaltis, and T. W. Hänsch, Opt. Lett. **29**, 772 (2004).
[10] H. F. Ghaemi *et al.*, Phys. Rev. B **58**, 6779 (1998).
[11] M. Sarrazin, J. P. Vigneron, and J. M. Vigoureux, Phys. Rev. B **67**, 085415 (2003).
[12] C. Genet, M. P. Van Exter, and J. P. Woerdman, Opt. Commun. **225**, 331 (2003).
[13] E. Altewischer, M. P. Van Exter, and J. P. Woerdman, J. Opt. Soc. Am. B **20**, 1927 (2003).
[14] K. Tetz, R. Rokitski, M. Nezhad, and Y. Fainman, Appl. Phys. Lett. **86**, 111110 (2005).
[15] K. Tetz, R. Rokitski, M. Nezhad, and Y. Fainman, in *Proceedings of the IEEE LEOS Annual Meeting 2004, Rio Grande, Puerto Rico* (IEEE, New York, 2004).
[16] A. Hohenau *et al.*, Opt. Lett. **30**, 893 (2005).
[17] M. L. M. Balistreri *et al.*, Science **294**, 1080 (2001).
[18] H. Gerson *et al.*, Phys. Rev. Lett. **94**, 073903 (2005).
[19] A. Nesci and Y. Fainman, Proc. SPIE-Int. Soc. Opt. Eng. **5181**, 62 (2003).